CORE
Metadata, citation and similar papers at core.ac.uk
Provided by Open Archive Toulouse Archive Ouverte

Open Archive TOULOUSE Archive Ouverte (OATAO)
OATAO is an open access repository that collects the work of Toulouse researchers and makes it freely available over the web where possible.

This is an author-deposited version published in : http://oatao.univ-toulouse.fr/
Eprints ID : 18112

To link to this article: DOI: 10.1007/s11085-017-9729-1
URL: http://dx.doi.org/10.1007/s11085-017-9729-1

To cite this version: Dupressoire, Charlotte and Rouaix - Vande Put, Aurélie and Emile, Philippe and Archambeau-Mirguet, Claude and Peraldi, Raphaëlle and Monceau, *Daniel Effect of nitrogen on the kinetics of oxide scale growth and of oxygen dissolution in the Ti6242S titanium-based alloy*. (2017) Oxidation of Metals, vol. 87 (n° 3-4). pp. 343-353. ISSN 0030-770X

Any correspondence concerning this service should be sent to the repository administrator: staff-oatao@listes-diff.inp-toulouse.fr

DOI 10.1007/s11085-017-9729-1

Effect of Nitrogen on the Kinetics of Oxide Scale Growth and of Oxygen Dissolution in the Ti6242S Titanium-Based Alloy

Charlotte Dupressoire[1,2] · Aurélie Rouaix-Vande Put[1] · Philippe Emile[2] · Claude Archambeau-Mirguet[2] · Raphaëlle Peraldi[2] · Daniel Monceau[1]

Abstract Titanium-based alloys are increasingly used in aircraft industry due to their good mechanical properties and low density. To reach better efficiencies, the engine design is constantly evolving and the temperature of the combustion chamber is always increasing. Then, surrounding parts are exposed to higher working temperatures and consequently have to cope with more severe oxidation phenomena. For Ti-based alloys, this leads to the formation of an external oxide scale and a large oxygen dissolution in the metal, which may be detrimental for ductility. As nitrogen is the major element of the atmosphere, it seems relevant to study its effect on the oxidation behavior of Ti-6Al-2Sn-4Zr-2Mo-0.1Si titanium-based alloy used for these applications. Thermogravimetric analyses were carried out at 650 °C for 100 h in synthetic air (20%O_2–80%N_2) and in a mixture of 20%O_2–80%Ar. Results showed that nitrogen decreases the oxidation kinetics by

✉ Charlotte Dupressoire
charlotte.dupressoire@ensiacet.fr

Aurélie Rouaix-Vande Put
aurelie.rouaix@ensiacet.fr

Philippe Emile
philippe.emile@airbus.com

Claude Archambeau-Mirguet
claude.archambeau@airbus.com

Raphaëlle Peraldi
raphaelle.peraldi@airbus.com

Daniel Monceau
daniel.monceau@ensiacet.fr

1 CIRIMAT, Université de Toulouse, CNRS, INPT, UPS, 4 allée Emile Monso, BP 44362, 31030 Toulouse Cedex 4, France

2 Airbus Operations SAS, 316 Route de Bayonne, 31060 Toulouse, France

slowing down the oxide scale growth but also by limiting the oxygen dissolution in the alloy.

Keywords Titanium-based alloys · Nitrogen · Oxidation kinetics · Oxygen dissolution

Introduction

Many studies were conducted on the oxidation of titanium and its alloys in air [1–8]. Several works, mostly on binary alloys, were performed using continuous thermogravimetric analyses and discontinuous weightings in both oxygen and air [1–4, 8]. They have shown that the mass changes followed similar evolutions in both atmospheres but that the mass gains in oxygen were higher than those in air. Apparent activation energies associated with the oxidation of titanium were measured as a function of time [3]. They were of the same order of magnitude for both environments. Besides, the stabilized value in air was very close to the activation energy corresponding to nitriding of titanium [9]. The following mechanism was proposed to explain the influence of nitrogen on oxidation [3]. At the early stages of oxidation, due to higher thermodynamic stability of oxides compared to nitrides, an oxide layer is formed on the surface. Then, nitrogen seems to be gradually incorporated to the rutile layer. As nitrogen has a higher diffusion coefficient in rutile and a slower dissolution in metal than oxygen [10, 11], it may accumulate in the oxide at the oxide–metal interface [3]. If nitrogen occupies anionic vacancies in the oxide, this would decrease the driving force for the oxygen diffusion in rutile and therefore the oxidation kinetics. Nitrogen dissolved in the metal may also reduce the oxygen concentration at the interface and then may slow down oxygen ingress in the Ti–O solid solution [3, 4]. Finally, at the oxide–metal interface, the oxygen partial pressure is low enough to favor nitride formation as seen for Ti–Cr and Ti–Si alloys where chromium and titanium nitrides were detected [1, 2] or as observed in TiAl and Ti_3Al alloys [12]. As Zr–O system is close to the Ti–O system, it is worth noting that nitrides and oxynitrides of zirconium were also detected, thanks to optical microscopy and Raman spectroscopy, at the oxide–alloy interface and sometimes in the oxide scale for Zircaloy-4 oxidized at 850 °C in oxygen and nitrogen mixtures [13]. However, no work on a fine characterization of the oxide–alloy interface was published in order to explain the effect of nitrogen on the oxidation kinetics. This would require quantifying the dissolution of nitrogen and oxygen in the alloy and to determine their thermodynamic interactions. In this study, both external oxide scale formation and oxygen dissolution in the alloy were examined by XRD, Raman and fluorescence spectroscopies, SEM, EPMA and Vickers microhardness measurements in order to determine its effect on the oxidation behavior of Ti6242S titanium-based alloy and especially to understand phenomena occurring at the oxide–alloy interface and just beneath it.

Experimental Procedures

Materials

The Ti6242S alloy of this study was supplied by Aubert and Duval (Pamiers, France). Its composition was determined by energy dispersive X-ray spectroscopy (EDX) for major elements and instrumental gas analyses (IGA) for gas-forming elements (detection limits: 5 ppm for nitrogen and 10 ppm for oxygen). It is given in Table 1.

The specimens used were thin plates of $15 \times 10 \times 1$ mm^3 cut from forged blocks. Before oxidation, all the specimens were mechanically polished using P240 SiC grinding paper and cleaned with acetone and ethanol under ultrasounds and weighed three times thanks to a SARTORIUS-GENIUS (ME2156P) balance whose accuracy was 20 μg.

Experiments and Characterization

The oxidation kinetics were determined with a SETARAM TAG24s thermobalance, which has an excellent mass stability over time (better than 1 μg/h) thanks to a symmetrical furnace design, and a mass variation sensibility equal to 0.1 μg. Isothermal oxidations were carried out at 650 °C for 100 h in two atmospheres (heating rates and initial cooling rates were 60 °C/min). Three samples were oxidized in each environment. The first environment was a bottled synthetic air (20%O_2–80%N_2). The second atmosphere was a 20%O_2–80%Ar gas mixture obtained by mixing the two gases with mass flow controllers. The flux was 8.5 mL/min corresponding to a gas velocity of 4.5×10^{-4} m/s. For the 20%O_2–80%Ar gas mixture, a vacuum of 10^{-1} mbar was reached in the reaction chamber before the gas mixture was introduced. All mass variations were corrected for buoyancy using the apparent mass variation during cooling to measure the buoyancy effect.

Oxide scales phases and compositions were determined thanks to X-ray diffraction (XRD) as well as Raman and fluorescence spectroscopies. XRD analyses were realized with a BRUKER D8-2 apparatus. Samples were characterized with a low incidence of 2°, a Bragg angle between 20 and 80° (in 2Θ), with a step of 0.04° and an acquisition time per step of 6 s. Raman and fluorescence analyses were carried out with a HORIBA YVON JOBIN HR 800 spectrometer equipped with a confocal microscope and a 532 nm laser. Optical observations were performed thanks to a MA200-NIKON microscope. The observation of the sample surface and cross section was carried out by scanning electron microscopy (SEM) with a LEO435VP microscope using the secondary electron mode (SE mode) and

Table 1 Chemical composition of the Ti6242S alloy

Chemical composition	Al	Sn	Zr	Mo	Si	Ti	*O*	*N*
Wt%	6.0	1.8	4.0	2.1	0.1	Bal.	1200 ppm	<5 ppm

the backscattered electron mode (BSE mode). Vickers microhardness profiles were obtained with a BUEHLER OMNIMET 2100 SERIE microhardness tester and using a 50-g diamond indent. Oxygen concentration profiles were measured by electron probe microanalyzer (EPMA) with a CAMECA SXFive microprobe working at 15 kV and 20 nA. Sample preparation was performed just before EPMA analyses to limit contamination and improve reproducibility. However, a correction was necessary. To do so, composition analyses were performed in the center of the oxidized samples by EPMA. A concentration of 5.2 wt% was obtained for oxygen while a concentration of 1200 mass ppm was measured by IGA. The EPMA values were then corrected by subtracting 5.08 wt% from oxygen concentration all over the concentration profile shown in Fig. 8. Uncertainties on the concentration measurements have been evaluated thanks to standard deviation to 0.9. Moreover, to avoid the influence of the oxide scale on the oxygen concentration measurement at the oxide–alloy interface, measurements were considered as accurate only if the concentrations of titanium and alloying elements were those of the bulk. Therefore, the first accurate oxygen concentrations were obtained at few micrometers from the interface.

Results and Discussion

Microstructure

The microstructure of the Ti6242S alloy was observed after etching with Kroll reactive (Fig. 1). Observations showed a duplex microstructure (also called bimodal microstructure) composed of lamellar and globular α-phases in a β-phase matrix.

Oxidation Kinetics

The mass changes obtained by thermogravimetry at 650 °C are shown in Fig. 2 for both environments. The general form of the curves was similar in both atmospheres. However, the mass gains in the 20%O_2–80%Ar mixture were around 2.5 times

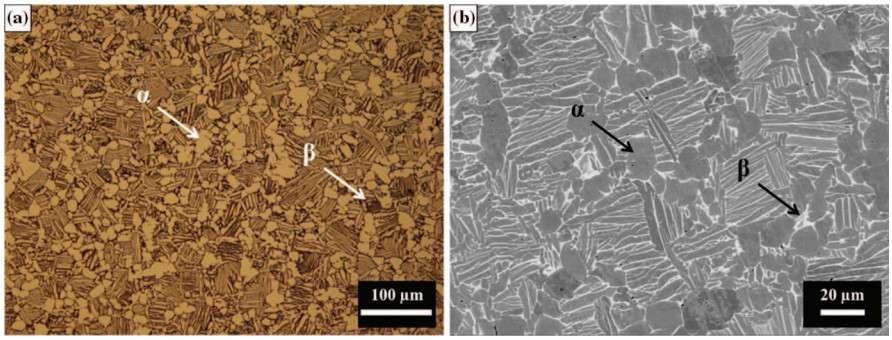

Fig. 1 Microstructure of the Ti6242S alloy: **a** optical observation and **b** SEM image (BSE mode)

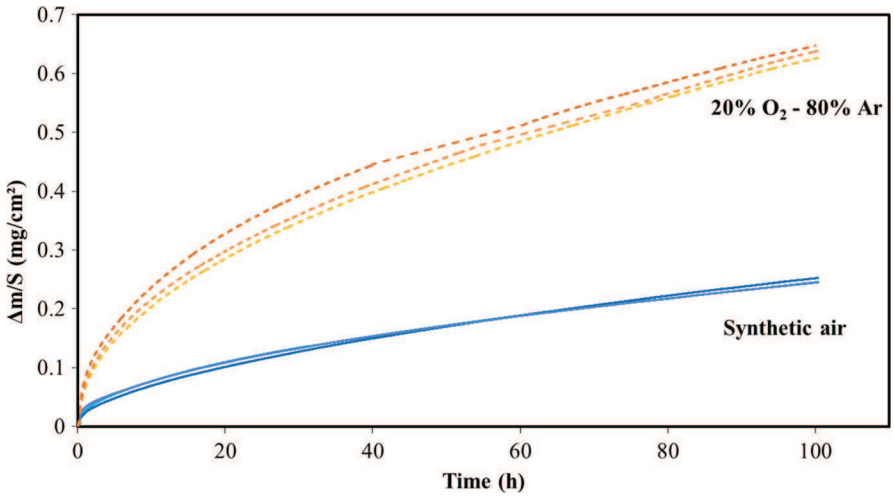

Fig. 2 Sample mass changes versus time for Ti6242S alloy oxidized at 650 °C for 100 h in both environments

Table 2 Parabolic rate constants, averaged on three oxidation tests performed at 650 °C for 100 h

Atmosphere	k_p ($\times 10^{-4}$ mg^2·cm^{-4}·h^{-1})
Synthetic air (20%O_2–80%N_2)	6.9 ± 1
20%O_2–80%Ar	36 ± 0.1

higher than those in synthetic air. Kinetics laws were parabolic in both cases. The parabolic rate constants were calculated using the complete parabolic law given by Eq. (1) [14]. A and B are coefficients obtained with the fit of the law whereas t, Δm and k_p are the time, mass gain and parabolic rate constant, respectively. The mean values for the three samples for each atmosphere are given in Table 2.

$$t = A + B\Delta m + \frac{1}{k_p}\Delta m^2 \tag{1}$$

Analyses of the Oxide Scale

The examination of the oxidized samples showed a difference of color depending on the atmosphere. Indeed, samples oxidized in synthetic air exhibited blue–green interference colors, whereas those oxidized in the oxygen–argon gas mixture had a gray oxide. This first examination was an insight of a thicker oxide scale in the case of oxidation in 20%O_2–80%Ar. Rutile and anatase TiO_2 were detected in the oxide scale by XRD (Fig. 3). It was confirmed by Raman spectroscopy (Fig. 4a). A small

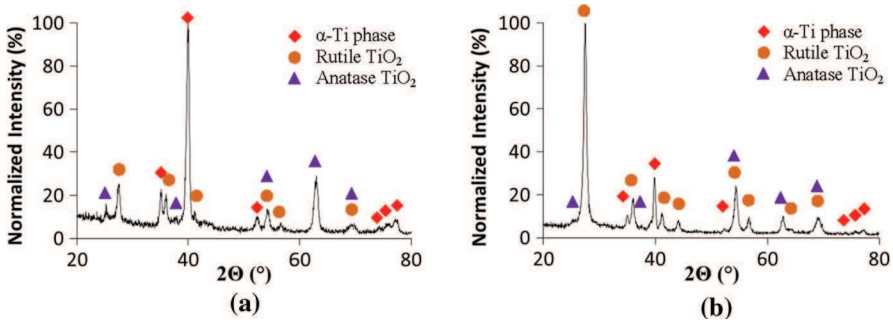

Fig. 3 XRD analyses with a low incidence angle of 2° for Ti6242S oxidized 100 h at 650 °C in **a** synthetic air and **b** 20%O_2-80%Ar

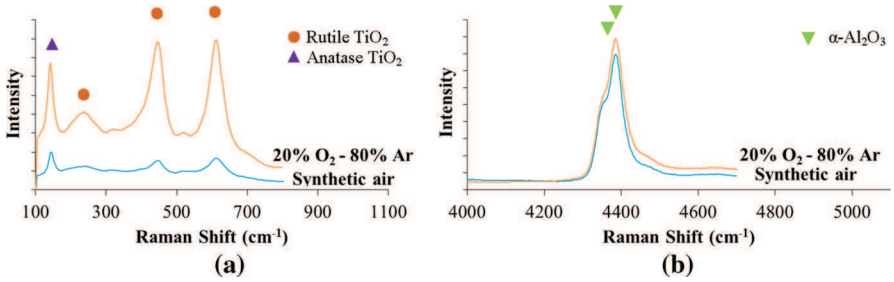

Fig. 4 **a** Raman and **b** fluorescence spectroscopy analyses of Ti6242S oxidized 100 h at 650 °C in both environments

quantity of α-Al_2O_3 also made up the oxide scale as it was identified by fluorescence spectroscopy (Fig. 4b) but not by XRD (Fig. 3). Their proportions varied depending on the atmosphere, as shown in Fig. 3.

According to XRD, Raman and fluorescence spectroscopy analyses, nitrogen did not have a noticeable effect on the oxide scale composition even if it seems that the

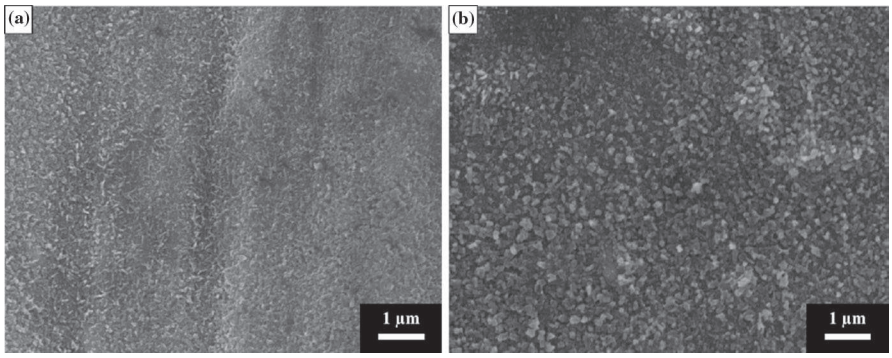

Fig. 5 SEM images (SE mode) of the surface of the oxide scale formed on the Ti6242S alloy **a** in synthetic air and **b** in 20%O_2–80%Ar after 100 h at 650 °C

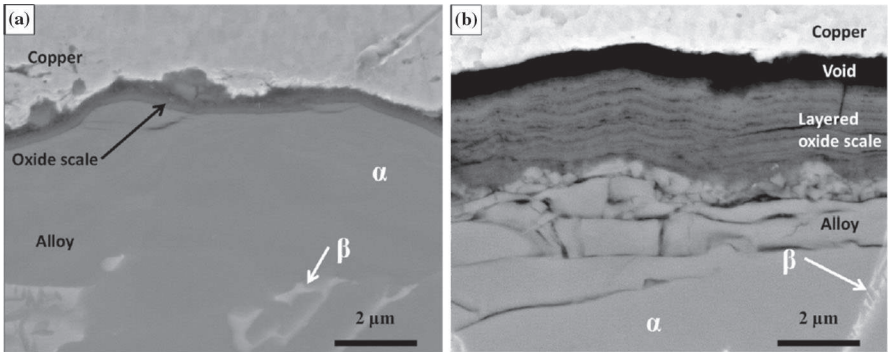

Fig. 6 SEM images (BSE mode) of the cross section of the oxide scale formed on the Ti6242S alloy **a** in synthetic air and **b** in 20%O_2-80%Ar after 100 h at 650 °C

rutile/anatase ratio decreased when the atmosphere contained nitrogen. Nevertheless, SEM observations revealed that it has a great influence on the oxide morphology (Figs. 5, 6). The oxide scale formed in synthetic air exhibited a needle-shaped morphology (Fig. 5a), whereas the one developed in the 20%O_2–80%Ar atmosphere presented equiaxed grains (Fig. 5b).

SEM observations of cross sections revealed large differences in the oxide scale morphologies depending on the atmosphere (Fig. 6). The oxide scale formed in synthetic air was composed of needles on top of a compact oxide layer (Fig. 6a). Its overall thickness was 280 ± 36 nm including the inner compact scale of approximately 140 nm. The oxide formed in 20%O_2–80%Ar atmosphere was very different with multilayered morphology and an external scale composed of equiaxed grains (Fig. 6b). An evaluation of the thickness of each layer was 250 nm, whereas the entire scale measured 1.5 ± 0.2 µm (average on eight measurements). It should be noticed that this layered morphology is a common feature for titanium oxide grown on pure titanium, as shown by Stringer [14]. In the case of pure titanium, the layering was explained by the presence of high stresses due to a large Pilling and Bedworth ratio (PBR). This ratio between the volume of the oxide and of the volume of the metal necessary to form the oxide is equal to 1.7 for the Ti/TiO_2 system. The layering usually leads to an increase in oxidation rate, with kinetics switching from parabolic to linear. However, the oxidation kinetics of Ti6242S in 20%O_2–80%Ar remained parabolic (Fig. 2). This means that the entire thickness of the scale was still acting as a diffusion barrier and that there was no direct access of the dioxygen gas to the alloy surface. The layering is supposed to start when a critical strain energy is built up, i.e., when a critical oxide scale thickness is reached. In our case, this critical thickness would be 250 nm. But the dense part of oxide scale formed in air is thinner than an individual layer grown in the O_2–Ar mixture. Therefore, it is not possible to know at this stage if the oxide scale formed in synthetic air will be layered or not for longer durations of oxidation.

Dissolution of Oxygen Within the Alloy

As titanium can dissolve oxygen up to 33 at.% [15], concentration of oxygen into the alloy and at the oxide–alloy interface is essential to understand diffusion phenomena and the influence of nitrogen on the oxidation behavior. Two Vickers microhardness profiles were made per sample to estimate the depth affected by oxygen diffusion. No significant difference was observed between samples oxidized with and without nitrogen (Fig. 7). However, the spatial resolution was not sufficient to measure hardness close enough to the oxide–alloy interface. Then, EPMA appeared to be more relevant. Analyses performed on samples oxidized in both atmospheres are shown in Fig. 8. The oxygen diffusion-affected depth was clearly smaller for samples oxidized in synthetic air than those oxidized in the 20%O_2–80%Ar gas mixture. The depth of the oxygen-affected zone was determined considering the depth where the oxygen concentration decreases down to 1200 mass ppm that is the oxygen concentration in the bulk. This zone measured around 8 μm and 14 μm for synthetic air and 20%O_2–80%Ar, respectively. Moreover, oxygen concentration close to the oxide–alloy interface was much higher in the 20%O_2–80%Ar atmosphere.

The mass gain associated with the oxygen dissolution into the alloy can be determined by calculating the area below the EPMA profiles. As the total mass gain is known, the mass gain associated with the formation of the oxide scale can then be deduced by difference and converted to a scale thickness. The obtained values are presented in Table 3. These calculations showed that both oxygen dissolution in the alloy and oxide scale thicknesses were smaller in synthetic air than in 20%O_2–

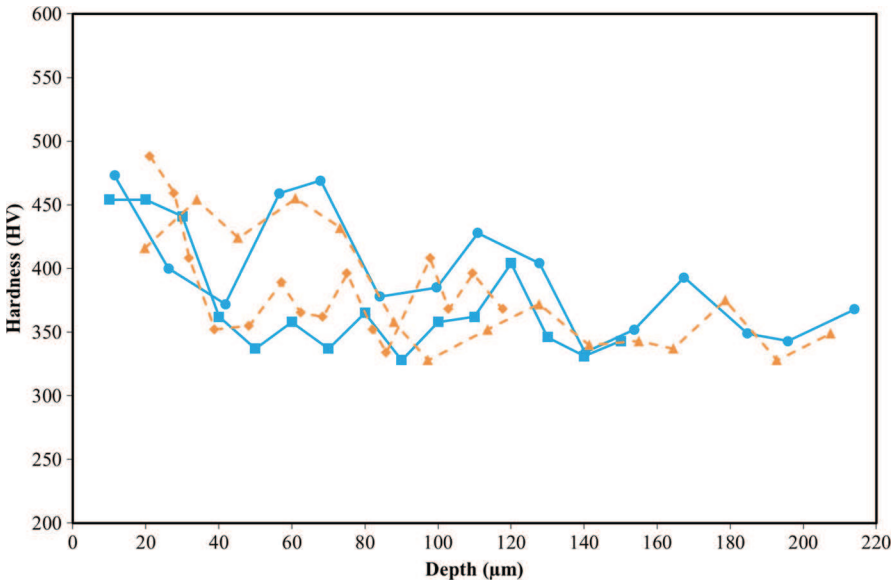

Fig. 7 Vickers microhardness profiles for Ti6242S oxidized at 650 °C for 100 h in synthetic air (*squares*, *circles* and *continuous lines*) and 20%O_2–80%Ar (*triangles*, *diamonds* and *dashed lines*)

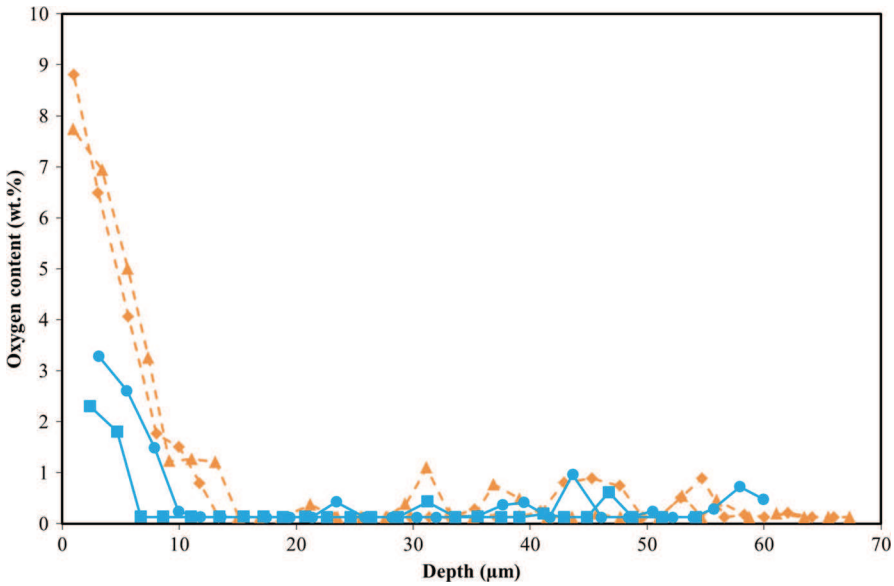

Fig. 8 EPMA profiles for oxygen for Ti6242S oxidized at 650 °C for 100 h in air (*squares*, *circles* and *continuous lines*) and 20%O_2–80%Ar (*triangles*, *diamonds* and *dashed lines*)

Table 3 Comparison of mass gains associated with the oxide formation $(\Delta m/S)_{ox}$ and with the oxygen dissolution in the alloy $(\Delta m/S)_{diss}$ with the global mass gain $(\Delta m/S)_{tot}$ (approximate values)

Atmosphere	$(\Delta m/S)_{tot}$ (mg/cm^2)	$(\Delta m/S)_{diss}$ (mg/cm^2) (EPMA)	$(\Delta m/S)_{ox}$ (mg/cm^2) By difference	$(\Delta m/S)_{diss}/(\Delta m/S)_{tot}$ (%)	Oxide scale thicknesses (nm)	
					Estimated with $(\Delta m/S)_{ox}$	Measured (MEB)
Synthetic air	0.263	0.106	0.157	40	930	280 ± 36
20%O_2–80%Ar	0.632	0.289	0.343	46	2020	1500 ± 200

80%Ar gas mixture. About 40–50% of the oxygen uptake corresponded to the oxygen dissolution in the alloy. This proportion is similar for both atmospheres. These results confirmed that nitrogen decreases oxygen dissolution and diffusion into the alloy. This is consistent with the previous mass gain measurements done on binary alloys by Chaze and Coddet [2, 3, 8, 16]. Nevertheless, one can remark in Table 3 that the calculated scale thicknesses are higher than the ones measured by SEM. This may be due to an underestimation of oxygen dissolution, because of the lack of spatial resolution of EPMA. The differences are too large to be explained by nitrogen dissolution. This could be also due to an underestimation of the oxide thickness by SEM, but it is not likely because no spallation was observed.

These authors proposed several hypotheses to explain the role of nitrogen. Three possible effects of nitrogen were stated. Two of them concerned the oxide scale thickness. First, nitrogen could reduce oxygen vacancies in the oxide scale at the oxide–metal interface where nitrogen is kinetically segregated because of its fast diffusion in the oxide scale and its slow ingress in the metal. This explanation is consistent with our observation of a thinner oxide scale in air, but nitrogen concentration measurements would be necessary in the oxide scale to be conclusive. It should be noticed that the effect of nitrogen on the vacancy concentration in rutile is controversial since recent studies indicate that oxygen vacancy formation is facilitated in nitrogen-doped TiO_2 [17, 18]. The second explanation concerns the oxide scale thickness as well as the oxygen dissolution in the metal. In the oxide scale, close to or at the oxide–metal interface, the oxygen partial pressure may be low enough to form nitrides or oxynitrides. These are well known to be diffusion barriers for the oxygen. Further analysis (transmission electron microscopy) is in progress to determine whether these phases are present, since they were not detected with SEM and EPMA. The third explanation concerned the oxygen dissolution in the alloy. If nitrogen is dissolved in the metal under the oxide scale, it is likely that it is competing with oxygen for interstitial sites in the titanium matrix. Therefore, one could think that nitrogen may reduce the oxygen dissolution in the metal. This would be consistent with our observations, i.e., with the lower oxygen concentration measured by EPMA in the metal at the oxide–metal interface. Analyses are in progress to measure the nitrogen content in the metal using another technique than EPMA which is not adapted. A final remark can be done from the observation of the oxide scale cross sections (Fig. 6). It can be seen that the metal has numerous cracks after sample preparation, below the oxide scale, for the sample oxidized in the 20%O_2–80%Ar mixture. This is a sign of the brittleness of the alloy enriched in oxygen, and it demonstrates the protection brought by nitrogen. It is also worth noting that this oxygen-enriched layer is strengthened by oxygen. The fact that the oxide scale grown without nitrogen is layered can be finally due to three different reasons: 1/its growth kinetics is faster, so there is less time for stress relaxation; 2/its substrate does not relax stresses because of strengthening by oxygen; and 3/the oxide scale does not reach the critical thickness of 250 nm. Longer experiments are underway to discuss these points.

Conclusion

Ti6242S Ti-based alloy was oxidized at 650 °C for 100 h in two oxidizing environments, 20%O_2–80%N_2 (synthetic air) and 20%O_2–80%Ar gas mixture, in order to study the effect of nitrogen independently of the oxygen partial pressure. It was shown that nitrogen decreases the oxidation kinetics of the titanium-based alloy. Firstly, XRD, Raman, fluorescence and SEM characterizations revealed that nitrogen has no noticeable effect on the oxide scale composition but a significant influence on the scale morphology by promoting needle formation. Secondly, it was shown that oxidation in the presence of nitrogen leads to a thinner and compact oxide scale, whereas the oxide scale formed without nitrogen was much thicker and

layered. It was shown also that nitrogen leads to a smaller amount of dissolved oxygen in the metallic substrate, as measured by EPMA. This last observation was the result of a smaller oxygen content at the oxide–alloy interface. Further work will now focus on a finer characterization of the oxidized samples in order to determine whether the effect of nitrogen is due to a decrease in the oxygen solubility in the metal and/or to nitride or oxynitride formation in the oxide scale or at the oxide scale interface.

Acknowledgments This work was supported by the French National Research Agency through the project ANR DUSTI in partnership between Airbus, Airbus Group Innovations, Aubert and Duval, Liebherr Toulouse Aerospace, Institut Pprime, Institut Jean Lamour and CIRIMAT Laboratory.

References

1. A. M. Chaze and C. Coddet, *Oxidation of Metals* **21**, 1984 (205).
2. A. M. Chaze and C. Coddet, *Oxidation of Metals* **27**, 1987 (1).
3. A. M. Chaze and C. Coddet, *Journal of the Less Common Metals* **124**, 1986 (73).
4. A. M. Chaze and C. Coddet, *Journal of Materials Science* **22**, 1987 (1206).
5. H. L. Du, P. K. Datta, D. B. Lewis and J. S. Burnellgray, *Corrosion Science* **36**, 1994 (631).
6. H. Guleryuz and H. Cimenoglu, *Journal of Alloys and Compounds* **472**, 2009 (241).
7. A. Ebach-Stahl, C. Eilers, N. Laska and R. Braun, *Surface & Coatings Technology* **223**, 2013 (24).
8. A. M. Chaze and C. Coddet, *Journal of the Less-Common Metals* **157**, 1990 (55).
9. K. N. Strafford and J. M. Towel, *Oxidation of Metals* **10**, 1976 (41).
10. D. David, G. Beranger and E. A. Garcia, *Journal of the Electrochemical Society* **130**, 1983 (1423).
11. C. J. Rosa, *Oxidation of Metals* **17**, 1982 (359).
12. J. Rakowski, D. Monceau, F. S. Pettit, G. H. Meier and R. A. Perkins, *Paper Presented at the Microscopy of Oxidation 2*, (Selwyn College, University of Cambridge, Cambridge, 1993).
13. M. Lasserre, V. Peres, M. Pijolat, J.-P. Mardon, *Journal of Nuclear Materials* **462**, 2015 (221).
14. D. Monceau and B. Pieraggi, *Oxidation of Metals* **50**, 1998 (477).
15. J. L. Murray and H. A. Wriedt, *Bulletin of Alloy Phase Diagrams* **8**, 1987 (148).
16. A. M. Chaze, C. Coddet and G. Béranger, *Journal of the Less Common Metals* **83**, 1982 (49).
17. X. Pan, M.-Q. Yang, X. Fu, N. Zhang and Y.-J. Xu, *Nanoscale* **5**, 2013 (3601).
18. Z. Zhang, et al., *Applied Catalysis, A: General* **425–426**, 2012 (117).